Journal of Fundamental and Applied Sciences

ISSN 1112-9867

Available online at http://www.jfas.info

Research Article

STRUCTURAL AND ELECTROCHEMICAL PROPERTIES OF Fe-DOPED $NiAl_2O_4$ OXIDES

W. Tibermacine, M. Omari*

University Mohamed Khider of Biskra, Laboratory of Molecular Chemistry and Environment, Faculty of Exact and Natural Sciences, 07000, Algeria

Received: 09 October 2018 / Accepted: 10 December 2018 / Published online: 01 January 2019

ABSTRACT

A new spinel solid solution system of $Ni_{1-x}Fe_xAl_2O_4$ ($0.0 \leq x \leq 0.5$) was synthesized through sol-gel method. The effect of Fe doping on the nickel aluminate prepared was investigated. The synthesized powders were characterized by means of X-ray diffraction, thermogravimetric and differential thermal analysis, fourier transform infrared spectroscopy, scanning electron microscopy and electrochemical measurements. From the preceding analysis, it can be shown that compounds show a single spinel phase in the temperature range 650-1000°C and the solubility of iron in the $NiAl_2O_4$ structure was limited to samples with the iron content $x < 0.6$. The electrochemical measurements indicate that the catalytic activity is strongly influenced by iron doping. The highest electrode performance is achieved with $Ni_{0.7}Fe_{0.3}Al_2O_4$ ($i=86.84$ mA/cm^2) which is ~ 27 times greater than that of $NiAl_2O_4$ ($i=3.22$ mA/cm^2) at $E= +0.8$V. After one hundred cycles, the stability of the doped electrode with 30% of iron is much better than the undoped electrode.

Keywords: Spinel oxide, Sol-gel, Powder diffraction, Thermal analysis, Oxygen evolution reaction.

Author Correspondence, e-mail: m2omari@yahoo.fr

doi: http://dx.doi.org/10.4314/jfas.v11i1.15

1. INTRODUCTION

Nanocrystalline metal aluminates possess important applications in various fields such as heterogeneous catalysis, pigments, sensors and ceramics [1-6]. Aluminate spinels have been used as catalysts in the decomposition of methane, steam reforming dehydration of saturated alcohols to olefins, dehydrogenation of alcohols, etc. These oxides have also been reported as good photocatalysts, e.g. for the degradation of methyl orange [7-12].

The general formula of spinels is AB_2O_4, they can be classified into three categories: normal, inverse, and intermediate. In the case of normal spinel, A^{2+} ions occupy tetrahedral sites and B^{3+} ions occupy octahedral sites. A^{2+} ions and $B3^{+}$ ions are surrounded by four and six oxygen ions, respectively. In the inverse spinel, the cation distribution occurs by inverted $(B)[AB]O_4$ arrangement, in which all the tetrahedral sites are occupied by B^{3+} cations, while an equal number of A^{2+} and B^{3+} cations share the octahedral sites. The intermediate spinel can be represented by $(A_{1-x}B_x)[A_xB_{2-x}]O_4$ formula, where x is the degree of inversion and $(A_{1-x}B_x)$, $[A_xB_{2-x}]$ represent the tetrahedral and octahedral sites, respectively [13,14] . It is known that the nature of occupancy of tetrahedral and octahedral sites depends on the calcination temperature [15]. Nickel aluminate ($NiAl_2O_4$) is a ternary oxide with AB_2O_4 spinel structure, where A and B are cations occupying tetrahedral (Ni^{2+}) and octahedral (Al^{3+}) sites, respectively [16]. Nickel aluminate has been used in various catalytic applications and high temperature fuel cells, due to its high melting point, high activity and resistance to corrosion[17]. It has been proposed as a promising candidate for an anode in aluminum production and as an anode in an internal reforming solid oxide fuel cell (IR-SOFC) [18,19], in addition it has been used as good electrocatalysts for the oxidation of organic compounds and nitrous oxide [10], and also as inert anodes in aluminum electrolysis [20]. On the other hand the spinel $NiAl_2O_4$ is photosensitive to visible light [21], and it presents an attractive property in photocatalysis [22,23].

This oxide can be properly modified by the partial substitution of atom at A and/ or B sites which may affect strongly its physical property. Nickel aluminate ($NiAl_2O_4$) oxide doped on the A site with various metal ions such as Cu [24], Cd [25], Mg [26], Ce [27], were previously studied. A few years ago, it has been reported that the oxygen evolution reaction (OER)

indicates that substitution of Ni by Fe in $Ni_{0.9}Fe_{0.1}Co_2O_4$ spinel increases the electrocatalytic activity of the resulting material significantly [28]. On the other hand, another work on mixed Fe-Ni oxide catalyst showed much higher activity toward oxygen evolution and methanol oxidation than either of the pure oxides with a peak in activity occurring near 10 mol % Fe [29]. In alkaline solution some substituted ferrites which the foreign element was added to the B site such as $CoFe_{1.7}Ni_{0.3}$ O_4 [30], $CoFe_{1.6}Mn_{0.4}O_4$ [30] and $NiFe_{2-x}Cr_xO_4$ ($0\leq x\leq 1$) [31], manifest a reduced oxygen over-potential.

Despite these advantages, there have been no reports to date concerning the synthesis and characterization of iron doped nickel aluminate oxides. In the present work, we examine the effect of partial substitution of nickel by iron on structural, grain morphology, surface area, optical and electrochemical properties of $Ni1_{-x}Fe_xAl_2O_4$ ($0\leq x\leq 0,6$) oxides prepared by the sol-gel method.

2. EXPERIMENTAL

2.1 Preparation of $Ni_{1-x}Fe_xAl_2O_4$ powders

Different nickel aluminate powders were prepared according to the formula $Ni_{1-x}Fe_xAl_2O_4$ ($0 \leq x \leq 0.6$) by a sol-gel process. $Fe(NO_3)_3.9H_2O$ (BIOCHEM), $Ni(NO_3)_2.6H_2O$ (BIOCHEM), $Al(NO_3)_3.9H_2O$ (FLUKA) and citric acid (JANSSEN CHIMICA) were used as salt precursors. The calculated amount of $Fe(NO_3)_3.9H_2O$, $Ni(NO_3)_2.6H_2O$, $Al(NO_3)_3.9H_2O$ was dissolved in C_2H_5OH 99%. Then, the proper amount of citric acid dissolved in ethanol was added where the mole ratio of total metal ions and citric acid is 1:2:3. The resulting solution was slowly stirred, heated and concentrated by evaporating the ethanol at 80°C until a gel was obtained. This last was then dried in an oven slowly upon increasing the temperature to 110°C for 12h in order to produce a solid amorphous citrate precursor. The resulting precursor was calcined in air for 6h in the temperature range 400-1000°C with a heating rate of 5°C min^{-1}.

2.2 Characterization

Thermal decomposition of the precursor was carried out using a SDT Q600 TA at a heating rate of 5°C min^{-1} in air. The Fourier transform infrared (FT-IR) absorption spectra were measured with FT-IR SHIMADZU 8400S infrared spectrophotometer. X-ray diffraction

(XRD) was performed with a D8 Advance Brucker using a Cu K_α line at 0.1540 nm in 2Θ range of 10°-90° in steps of 0.010°. Morphological aspect of the powders was examined by using a ESEM-FEI Quanta 250 scanning electron microscope. The specific surface area of the samples (S_{BET}) was determined by applying the BET method to nitrogen adsorption /desorption isotherms recorded at (-196°C) using a Micromeritics ASAP 2020 Analyzer. Linear sweep and cyclic voltammetry experiments for O_2 evolution were performed in potassium hydroxide 1M using a Parstat 4000 potentiostat-galvanostat with oxide powders , Pt plate and Hg/HgO as working, auxiliary and reference electrodes, respectively.

2. RESULTS AND DISCUSSION

3.1 TG-DTA analysis

The precursor was examined by TGA-DTA in order to explore its decomposition under atmospheric air and with the aim of establishing most adequate calcination conditions for it. The results of $Ni_{0.8}Fe_{0.2}Al_2O_4$ analysis are shown in Fig.1. Basically, the TGA curve exhibits four weight loss stages and the DTA curve exhibits one broad endothermic peak and three exothermic peaks. In the first temperature region up to ca.180°C, a low weight loss of about (5.10 %) accompanying with a broad endothermic peak at T~110°C which must be related to the desorption of adsorbed or hydration water may remain in the precursor [32-34]. A great reduction in weight (43,87%) observed in the temperature range 180-325°C corresponding to an exothermic process, can be ascribed to the oxidative decomposition of citrates complexing the metals in the precursor [32]. The temperature region between ca. 325 and 600°C with one exothermic peak and a mass loss of about (21,44%) can be assigned to the formation of nickel oxide [35]. Further heating (T> 600°C), a slight weight loss of about (2,57%) correlates with one small exothermic peak taking place up to ca. 800°C , can be attributed to the final decomposition of nickel oxide and formation of $Ni_{0.8}Fe_{0.2}Al_2O_4$ oxide. After 800°C, we find no weight loss and stabilization of the DTA curve, indicating that the final crystallization process of $Ni_{0.8}Fe_{0.2}Al_2O_4$ cristal, as was confirmed by XRD results, discussed below.

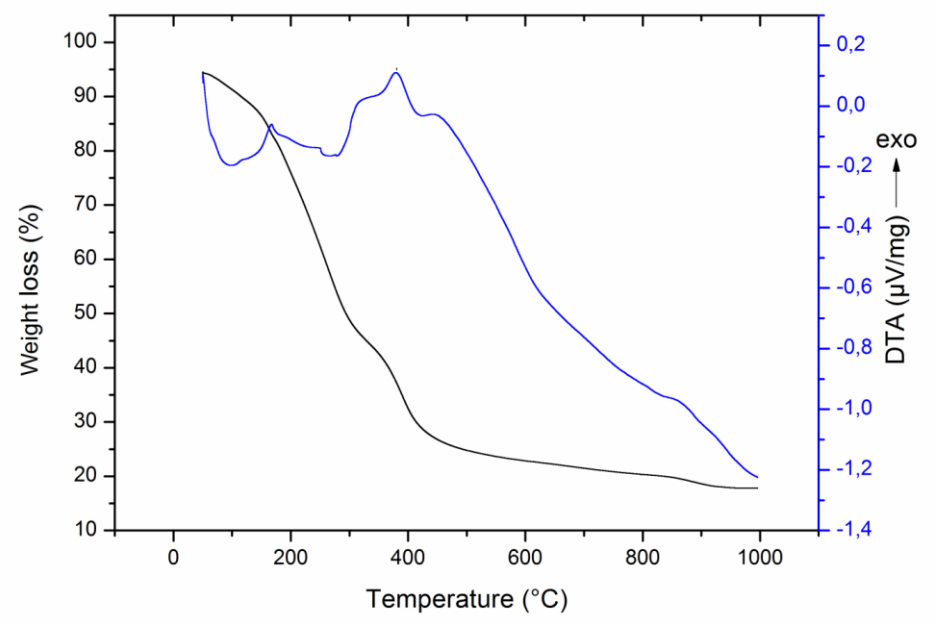

Fig.1. TG and DTA curves of $Ni_{0.8}Fe_{0.2}Al_2O_4$ precursor heated in air at 5°C min^{-1}

3.2 XRD study

The XRD patterns of the $Ni_{1-x}Fe_xAl_2O_4$ (x=0, 0.1, 0.2, 0.3, 0.4, 0.5 and 0.6) calcined at 650-1000°C for 6h in air are shown in Figure 2. The results confirm that all samples with $0 \leq x \leq 0.5$ are consistent with the standard data for $NiAl_2O_4$ spinel phase (JCPDS card No. 10-0339), indicating the formation of single phase with space group Fd3m and with no detectable secondary phase. These peaks can be indexed as (111), (220), (311), (400), (422), (511), and (440) plane, respectively. These planes are associated with the nickel aluminate spinel with cubic structure. For x=0.6, the main phase was also cubic spinel with another phase $FeAl_2O_4$ (JCPDS card 00-007-0068) indicating a Fe solubility limit of ~ 0.5 in the $Ni_{1-x}Fe_xAl_2O_4$.

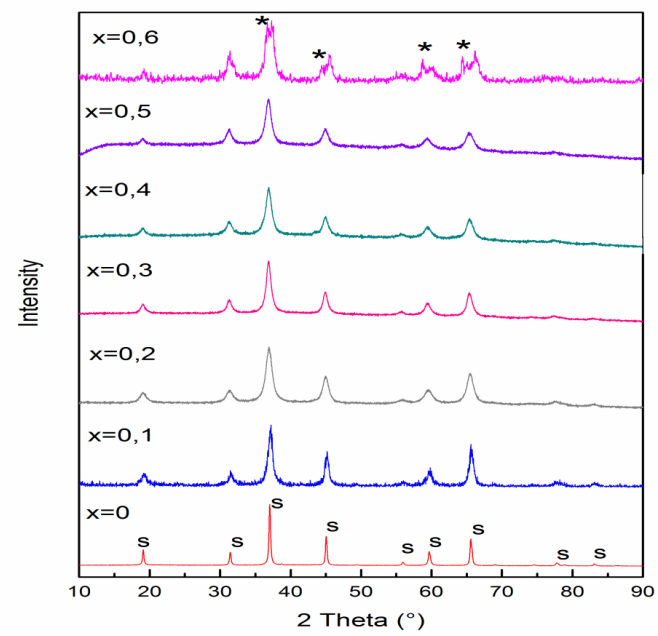

Fig.2. XRD patterns of the $Ni_{1-x}Fe_xAl_2O_4$ ($0 \leq x \leq 0.6$) samples calcined at (650-1000°C)

(s) : spinel ; (*) : $FeAl_2O_4$

Figure 3 shows the most intensive diffraction peak of Fe- doped $NiAl_2O_4$, with 2θ around 37.02° , indexed to the (311) reflection of the cubic spinel structure. This peak shifts to lower angles with increasing Fe content. The phase compositions, lattice parameters and unit cell volumes of the investigated samples $0 \leq x \leq 0.5$ after heat treatment at (650-1000°C) are summarized in table 1. The lattice parameters of the spinel increase slightly with increasing x from 0 to 0.5. Similar tendency has been found previously for $Ni_{0.9}Fe_{0.1}Co_2O_4$ samples [28].

Table 1. Values of unit cell parameters for pure and substituted $NiAl_2O_4$

Fe content	A= B =C (Å)	V (Å^3)
X=0	8.04775	521.222
X=0.1	8.06155	523.908
X=0.2	8.05829	523.273
X=0.3	8.07310	526.163
X=0.4	8.08787	529.057
X=0.5	8.07435	526.408

This is due probably to the substitution of Ni^{2+} by Fe^{2+} in tetrahedral coordination and the substitution of Al^{3+} by Fe^{3+} in octahedral coordination. Another similar result was also found

in $Co_{1-x}Fe_xCr_2O_4$ solid solution [36]. It has been reported that trivalent Fe ions can substitute Cr^{3+} in octahedral positions while bivalent Fe ions substitute Co^{2+} in tetrahedral positions which indicates that the spinel samples solid solution are a partly inverse type [37].

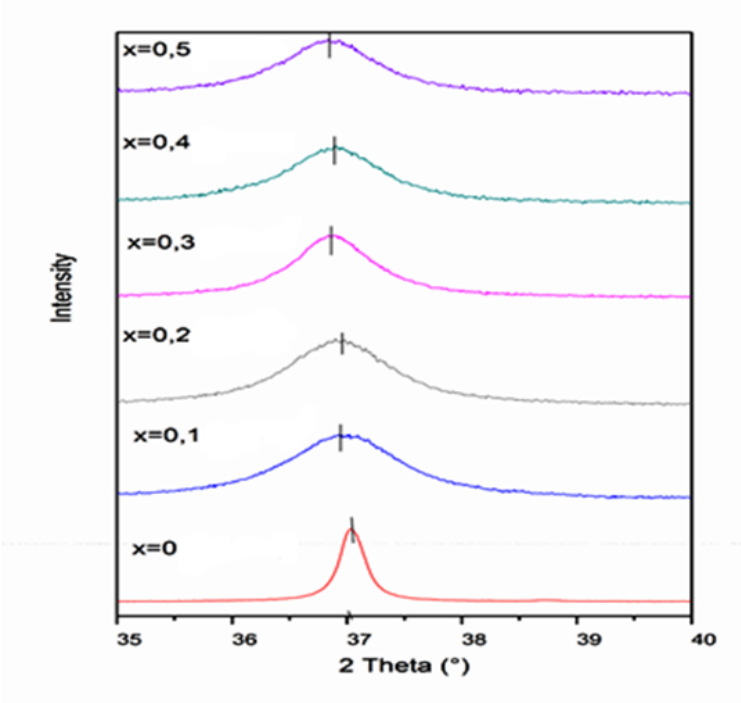

Fig.3. Evolution of the position of the highest X-ray diffraction peak

Figure 4(a, b) shows the DRX patterns of $NiAl_2O_4$ and $Ni_{0.8}Fe_{0.2}Al_2O_4$ respectively calcined at different temperatures for 6h. After calcination in the temperature range 400-600°C, the precursor $NiAl_2O_4$ exhibits a single rhombohedral phase NiO (PDF: 00-022-1189). When the precursor was heated at 800, 900°C the characteristic diffraction peaks of NiO become weaker while those of spinel structure $NiAl_2O_4$ appear at 800°C and become stronger at 900°C. With the increase of calcination temperature at 1000°C, the characteristic diffraction peaks of NiO disappear while intensity of characteristic diffraction peaks of spinel structure $NiAl_2O_4$ shows a good crystallinity. For the precursor $Ni_{0.8}Fe_{0.2}Al_2O_4$, the single phase of NiO appears in the temperature range 400-500°C. After calcination at 600°C the characteristic diffraction peaks of the spinel structure of $Ni_{0.8}Fe_{0.2}Al_2O_4$ appear while those of NiO become weaker. With the increase of calcination temperature from 800°C to 1000°C the precursor shows an increasing in crystallinity and a thermal stability of the pure spinel structure of $Ni_{0.8}Fe_{0.2}Al_2O_4$. This is consistent with TGA-DTA analysis which confirms that the final

crystallization process becomes shifted to low temperature in the presence of iron.

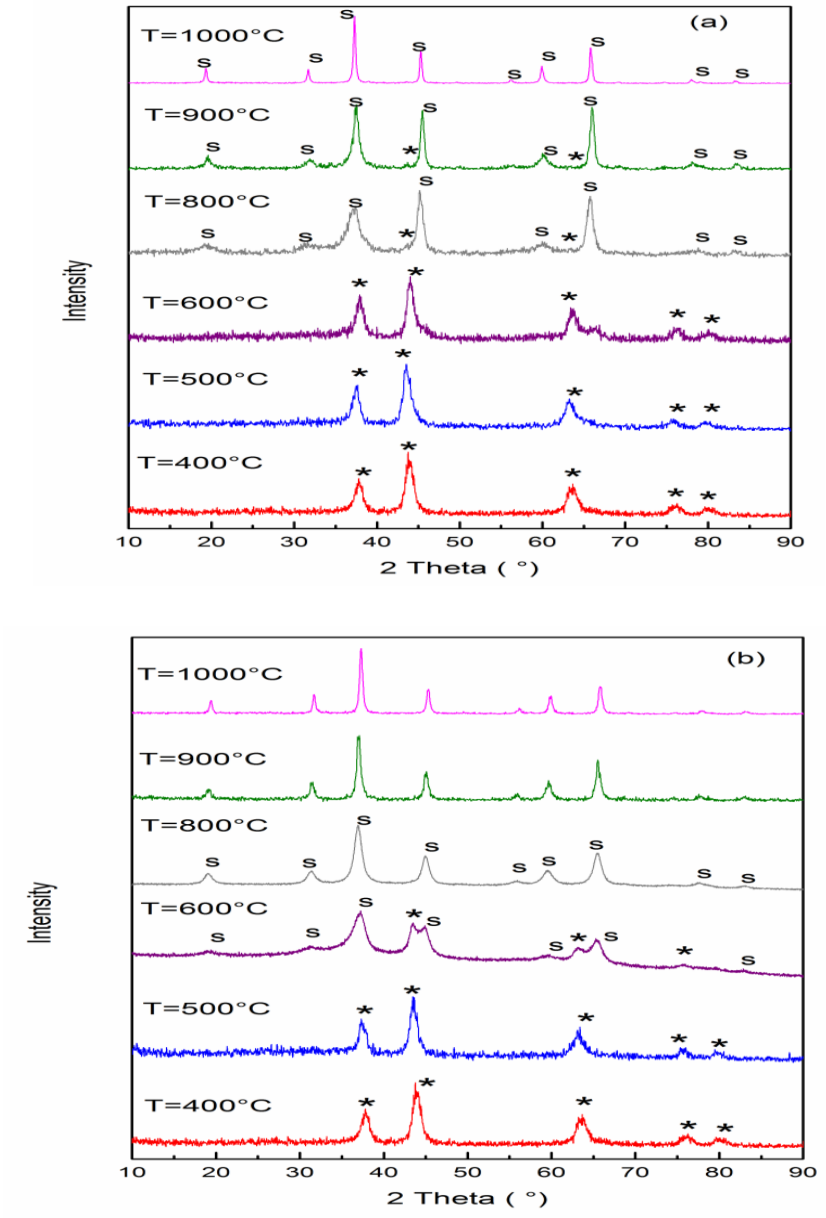

Fig.4. X- ray diffractograms heating at different temperatures (a): $NiAl_2O_4$; (b) : $Ni_{0.8}Fe_{0.2}Al_2O_4$. (s) : spinel phase ; (*) : NiO

3.3 FT-IR spectra

The $Ni_{1-x}Fe_xAl_2O_4$ $(0 \leq x \leq 0.5)$ samples have been explored by infrared spectroscopy. As shown in Fig. 5, crystallized powders $Ni_{1-x}Fe_xAl_2O_4$ show metal-oxygen stretching frequencies in the range 500-900 cm^{-1} associated with the vibrations of M-O, Al-O and

M-O-Al bands [5, 38]. Two characteristics bands of the spinel phase at approximately 500 and 728 cm^{-1} [5, 39], were observed. The peak at 500 cm^{-1} was associated with the stretching vibration mode of Al-O for the octahedral coordinated Al^{3+} ions [40]. The band at 728 cm^{-1} corresponds to lattice vibrations of the tetrahedral coordinate Al-O [41]. These results are consistent with the crystallization process observed by TG/DTA and XRD measurements.

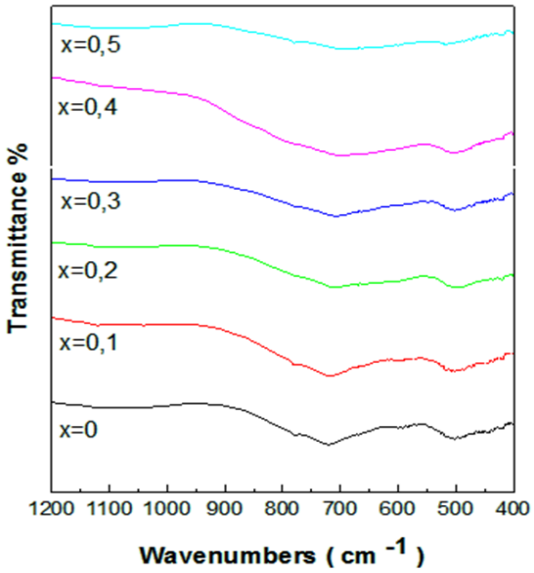

Fig.5. Infrared spectra of $Ni_{1-x}Fe_xAl_2O_4$ $0.0 \leq x \leq 0.5$ samples calcined at (650-1000°C)

3.4 SEM analysis

The crystallite size (Dhkl) of the samples $0 \leq x \leq 0.5$ was calculated using Scherrer's equation (Eq. 1) [42].

$$D = k\lambda / \beta \cos\theta \qquad (1)$$

Where D is the average size of crystallites (nm) , k Scherrer constant (≈0.9), λ wavelength of the incident radiation (nm), θ half of the angular position of the peak concerned and β full width at half maximum.

Fig.6 presents the crystallite size for different compositions in the range of 13.4-43nm indicating that the spinel powders prepared by sol-gel method are composed of nanometric particles. The crystallite size decreases with increasing iron content. A similar result was also found for $Ni_{0.9}Fe_{0.1}Co_2O_4$ [28].This is probably due to the incorporation of iron into the $NiAl_2O_4$ lattice, which leads to the formation of either cation or oxygen vacancies reducing the crystallite size.

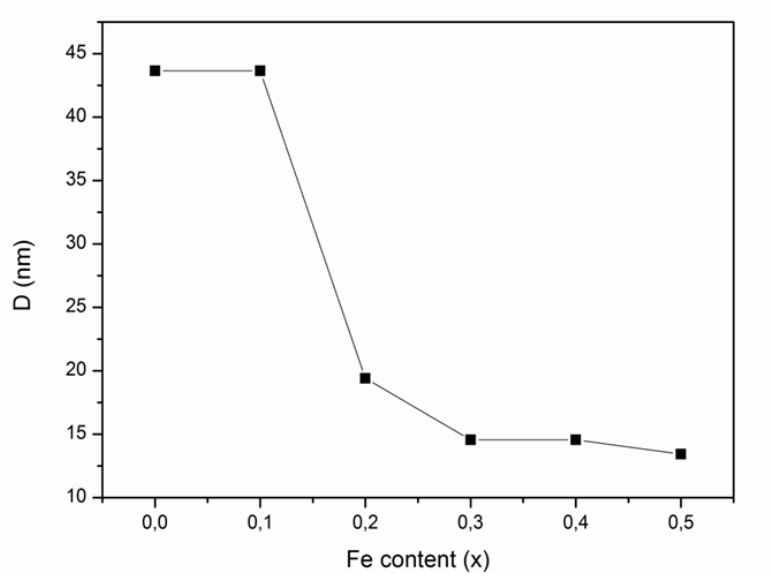

Fig.6. Crystallite size of $Ni_{1-x}Fe_xAl_2O_4$ ($0.0 \leq x \leq 0.5$) samples

The SEM micrographs of $Ni1_{-x}Fe_xAl_2O_4$ samples are shown in Fig. 7 (a-f). Particles have different shapes, sizes and the powders are agglomerated. The particle size is appreciated between 0.6 and 2.3µm. The formation of agglomerate is probably due to the nature of the solvent used in the preparation of samples [43]. Table 2 summarizes the basic textural properties of the samples. As noted, the specific surface area increases with increasing of Fe content and decreasing of calcination temperature. As expected, when the temperature of calcination decreases, the surface areas are rather high due to the lower crystallinity of the spinel and/or the decrease in the particle size. This result was expected since the calcination promotes the sintering of crystallites, which produces materials with lower surface area [44].

Table 2 Main textural properties of $Ni_{1-x}Fe_xAl_2O_4$ samples calcined at (650-1000° C)

$Ni_{1-x}Fe_xAl_2O_4$	Surface BET (m^2/g)	Pore volume (cm^3/g)	Average pore diameter (Å)
X=0	7.89	0.0211	101.9
X=0.1	21.79	0.0439	49.1
X=0.2	39.49	0.0728	52.4
X=0.3	43.12	0.1103	73.4
X=0.4	51.36	0.1095	57.7
X=0.5	54.15	0.1232	63.4

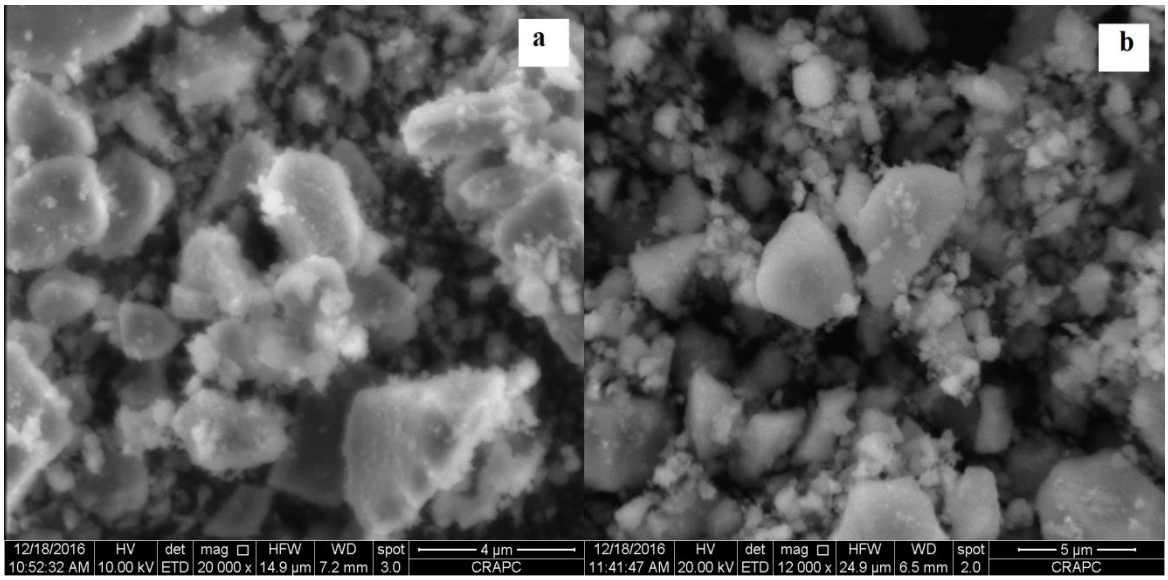
a
b
12/18/2016 10:52:32 AM HV 10.00 kV det ETD mag 20 000 x HFW 14.9 µm WD 7.2 mm spot 3.0 4 µm CRAPC
12/18/2016 11:41:47 AM HV 20.00 kV det ETD mag 12 000 x HFW 24.9 µm WD 6.5 mm spot 2.0 5 µm CRAPC

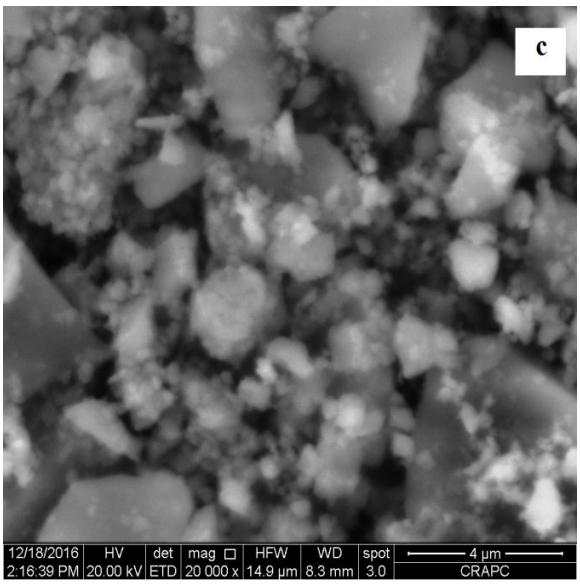
c
12/18/2016 2:16:39 PM HV 20.00 kV det ETD mag 20 000 x HFW 14.9 µm WD 8.3 mm spot 3.0 4 µm CRAPC

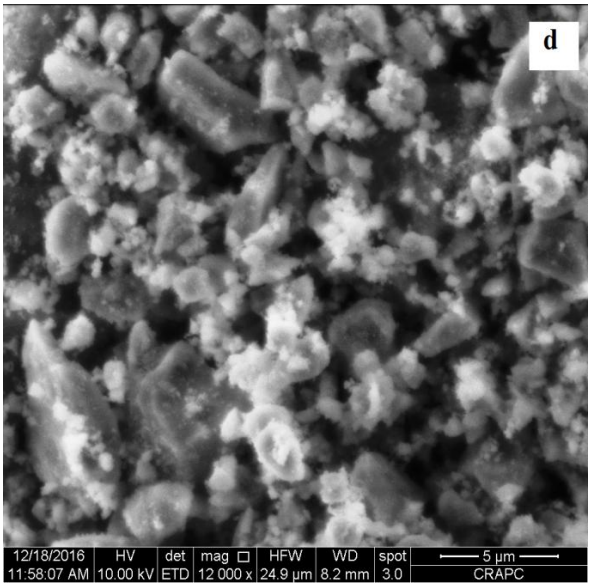
d
12/18/2016 11:58:07 AM HV 10.00 kV det ETD mag 12 000 x HFW 24.9 µm WD 8.2 mm spot 3.0 5 µm CRAPC

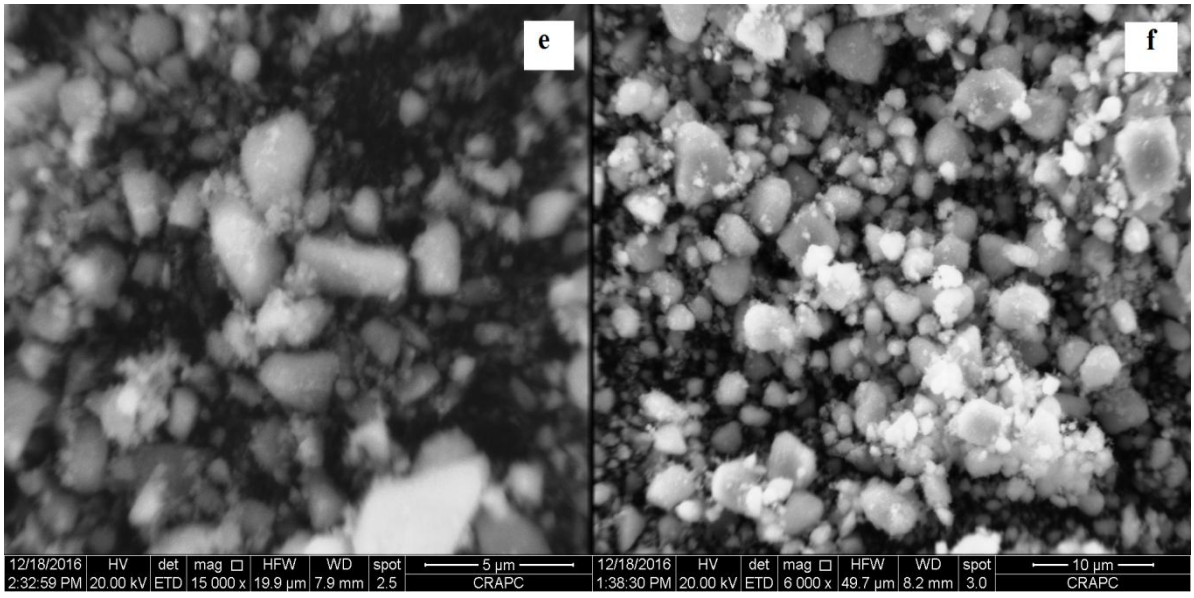

Fig.7. SEM micrographs of $Ni_{1-x}Fe_xAl_2O_4$.(**a) :** x=0; (**b) :** x =0.1; (**c) :** x=0.2; (**d) :** x=0.3 ; (**e) :** x =0.4 ; (**f) :** x=0.5 calcined at (650-1000°C)

3.5 Electrochemical properties

3.5.1 Catalytic activity of $Ni_{1-x}Fe_xAl_2O_4$ electrodes

Polarization studies under potentiostatic conditions for $Ni_{1-x}Fe_xAl_2O_4$ ($0 \leq x \leq 0.5$) catalysts were carried out (Fig. 10). The highest electrode performance is achieved, for anodic current density with $Ni_{0.7}Fe_{0.3}Al_2O_4$. Oxygen evolution reaction shows an important jump for ($0.0 \leq x \leq 0.3$), where the current density of Ni0.7Fe0.3Al2O4 (i=86.84 mA/cm^2) is ~ 27 times greater than that of $NiAl_2O_4$ (i=3.22 mA/cm^2) at E= +0.8V. As Fe content is increased beyond 30 %, catalytic activity starts to decrease. The improvement of catalytic activity with incorporation of iron ($x \leq 0.3$) is probably due to the amelioration of the conductivity and the crystallinity of the doped material [45-46]. Burke et al. have also reported the role of iron in activating OER catalysts [47]. It has been shown that oxidized nickel (oxy) hydroxide is conductive and thus electrically connects the dispersed Fe sites to the conductive electrode. On the other hand, the electronic interaction between Ni and Fe likely further activates the Fe site for the OER. For higher iron content ($x > 0.3$), the trend reverses and the catalytic activity becomes lower. This can be probably due to that these catalysts have not the optimal M-O bond strength that is this bond which constitutes intermediate specie of the OER mechanism is too strong or too weak.

On the other side, Friebel et al. [48] have reported that for Fe content 25-50%, the presence of the phase-segregated FeOOH that lowered the overall geometric activity. This is due to that FeOOH is electrically insulating and thus OER is less active [47].

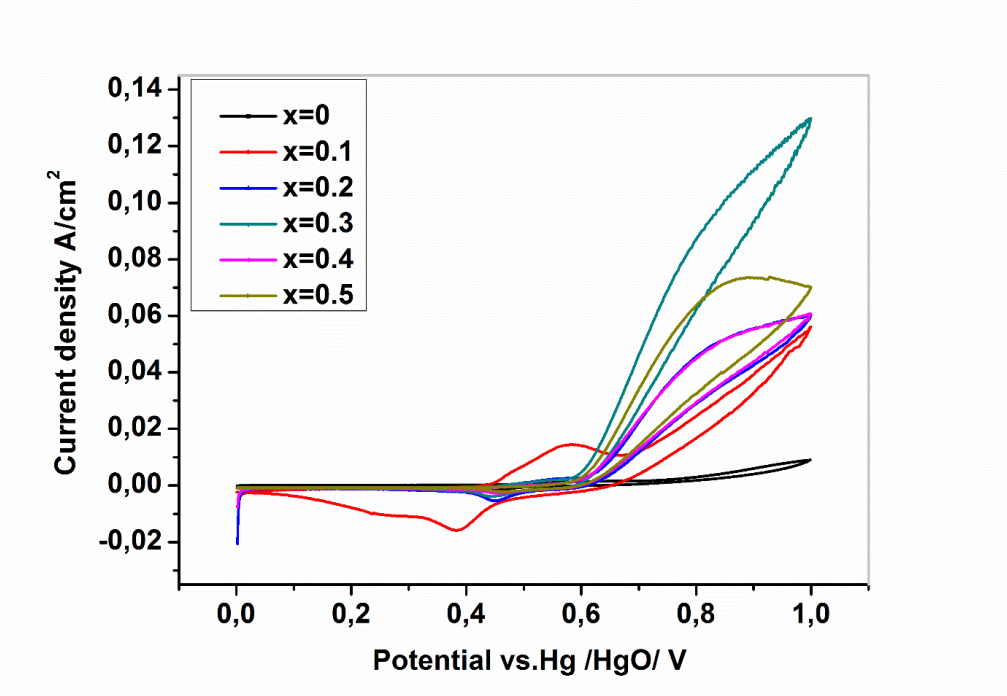

Fig.8. i–E polarization curves of oxygen evolution reaction of $Ni_{1-x}Fe_xAl_2O_4$ electrodes in 1M KOH

3.5.1 Stability of $Ni_{1-x}Fe_xAl_2O_4$ electrodes.

The $Ni_{1-x}Fe_xAl_2O_4$ oxides stability under oxygen evolution reaction conditions was tested. Figure 9 shows the cyclic voltammograms of the 1st and 100th cycle for $NiFeAl_2O_4$ and $Ni_{0.7}Fe_{0.3}Al_2O_4$ electrodes towards oxygen evolution reaction. In the two cases, after one hundred cycles, the curves show almost similar peaks with a slight decrease in current density for the undoped sample while it becomes higher for $Ni_{0.7}Fe_{0.3}Al_2O_4$ at E > 0.7V. Indeed, during 100 cycles, the current density decreases from 3.22 to 2.11 mA/cm^2 (~ 34%) for $NiFeAl_2O_4$ and increases from 86.84 to 91.75 mA/cm^2 for $Ni_{0.7}Fe_{0.3}Al_2O_4$ (~ 5.65%) at E=0.8V. This result indicates clearly that the stability of the electrode doped with 30% of iron is much better than the undoped electrode. This is probably due to the improved crystallinity of the doped sample compared to the undoped one [49]. Furthermore the current density of

$Ni_{0.7}Fe_{0.3}Al_2O_4$ electrode after 100 cycles is 5.65 % higher than that of the first cycle indicating that this electrode is more activated which explains its better catalytic activity.

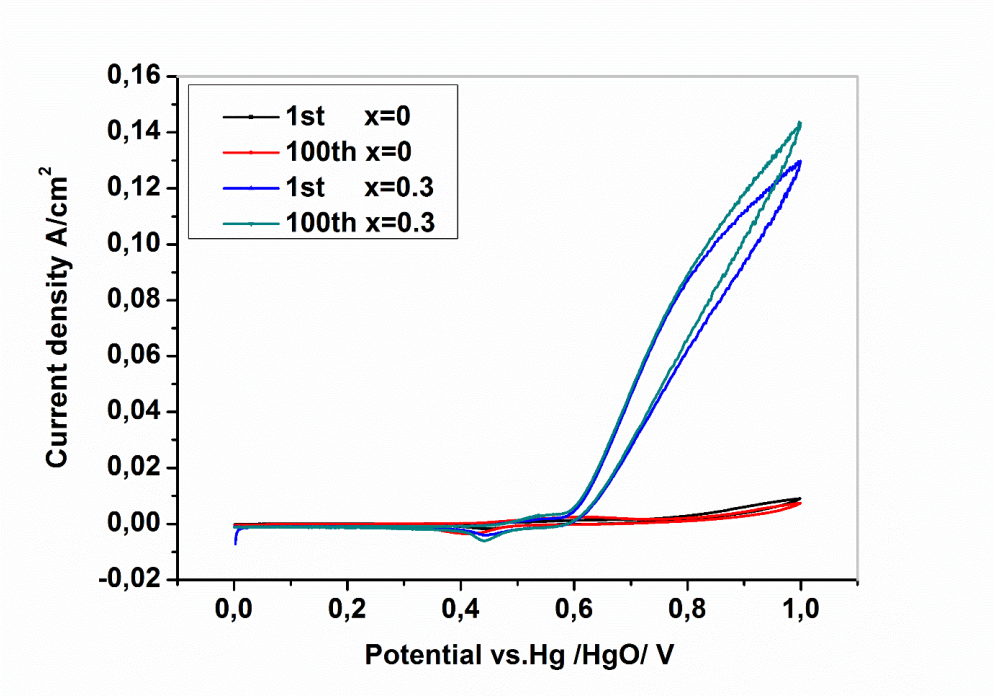

Fig.9. Cyclic voltammograms of $NiFeAl_2O_4$ and $Ni_{0.7}Fe_{0.3}Al_2O_4$ for the 1st and 100th cycles in 1M KOH media

4. CONCLUSION

The $Ni1_{-x}Fe_xAl_2O_4$, ($0 \leq x \leq 0.5$) spinel oxides were prepared via sol-gel method. XRD analysis reveals that all samples crystallize with cubic structure at the temperature range (650-1000°C), as well confirmed by IR spectroscopy. A single-phase structure was observed for $Ni1_{-x}Fe_xAl_2O_4$ at $0 \leq x \leq 0.5$. The microstructure of the compounds show that particles are partially spherical in shape and the powders are partially agglomerated.

The electrochemical behavior of these samples reveals that the electrode with 30% of iron content $Ni_{0.7}Fe_{0.3}Al_2O_4$ exhibits a higher electroactivity. This indicates that Ni0.7Fe0.3Al2O4 oxide is among the investigated series the best electrocatalyst for oxygen evolution reaction. These results show clearly that there is a close relationship between the activity of the catalyst and the iron content. After one hundred cycles, the stability of the doped electrode with 30% of iron is much better than the undoped one. The catalytic activity is improved with ~ 5.65%

for $Ni_{0.7}Fe_{0.3}Al_2O_4$ while it is reduced with ~ 34% for $NiFeAl_2O_4$.

5. REFERENCES

[1] Dhak D, Pramanik P, J. Am. Ceram. Soc. 89, 2006, 1014-1021, doi.org/10.1111/j.1551-2916.2005.00769.x

[2] Feldmann C, Adv.Mater. 13, 2001, 1301-1303, doi.org/10.1002/1521-4095.

[3] Michel CR, Sensors Actuators B Chem. 147, 2010, 635- 641, doi.org/10.1016/j.snb.2010.04.013

[4] Michel CR, Rivera J, Martinez AH, Santana-Aranda M, J. Electrochem. Soc.155, 2008, 263-269, doi: 10.1149/1.2956971.

[5] Cavalcante PMT, Dondi M, Guarini G, Raimondo M, Baldi G, Dye. Pigment 80, 2009, 226- 232, doi.org/10.1016/j.dyepig.2008.07.004.

[6] Lorenzelli V, Escribano VS, Guidetti R, J. Catal. 131, 1991,167-177, doi.org/10.1016/0021-9517(91)90333-Y

[7] Dussault L, Dupin J-C, Guimon C, Monthioux M, Latorre N, Ubieto T, Romeo E, Royo C, Monzon A, J. Catal. 251, 2007 223-232, doi.org/10.1016/j.jcat.2007.06.022

[8] Salhi N, Boulahouache A, Petit C, Kiennemann A, Rabia C, Int. J. Hydrogen Energy 36, 2011, 11433- 11439, doi.org/10.1016/j.ijhydene.2010.11.071

[9] Nakka L, Molinari JE, Wachs IE, J. Am. Chem.Soc. 131, 2009, 15544- 15554, doi: 10.1021/ja904957d

[10] Cesteros Y, Salagre P, Medina F, Sueiras J.E, Appl. Catal. B Environ. 25, 2000, 213-227, doi.org/10.1016/S0926-3373(99)00133-2

[11] Ribeiro NFP, Neto RCR, Moya SF, Souza MMVM, Schmal M, Int. J. Hydrogen Energy, 35, 2010, 11725- 11732, doi.org/10.1016/j.ijhydene.2010.08.024

[12] Lu W, Liu B, Qiu Q, Wang F, Luo Z, Zhang P, J. Alloys Compd. 479, 2009,480-483, doi.org/10.1016/j.jallcom.2008.12.111

[13] Poleti D, Vasović D, Karanović L, Branković Z, J. Solid State Chem. 112, 1994, 39-44, doi.org/10.1006/jssc.1994.1261

[14] Souza LKC, Zamian JR, Filho GNR, Soledade LEB, Santos IMG, Souza AG, Scheller T,

Angélica RS, Costa CEF, Dye. Pigm. 81, 2009, 187- 192, doi.org/10.1016/j.dyepig.2008.09.017

[15] Cimino A, Lo Jacono M, Schiavello M, J. Phys. Chem. 75, 1971, 1044-1050, doi: 10.1021/j100678a005

[16] Han YS, Li JB; Ning XS, Yang XZ, Chi B, Mater. Sci. Eng. A 369, 2004, 241-244, doi.org/10.1016/j.msea.2003.11.026

[17] Nazemi MK, Sheibani S, Rashchi F, Gonzalez-DelaCruz VM, Caballero A, Adv. Powder Technol. 23, 2012, 833-838, doi.org/10.1016/j.apt.2011.11.004

[18] Peelamedu RD, Roy R, Agrawal DK, Mater. Lett. 55, 2002, 234-240, doi.org/10.1016/S0167-577X(01)00653-X

[19] Han YS, Li JB, Ning XS, Chi B, J.Am. Ceram. Soc. 88, 2005, 3455-3457, doi.org/10.1016/S0167-577X(01)00653-X

[20] Jentoftsen T.E, Lorentsen O, Dewing E.W, Haarbeg J.M, Thonstad J, Metall. Mater. Trans. B 33, 2002, 901-908, doi.org/10.1007/s11663-002-0073-7

[21] Sebai I, Salhi N, Rekhila G, Trari M, Int. J. Hydrogen Energy 42, 2017, 26652-26658, doi.org/10.1016/j.ijhydene.2017.09.092

[22] Yang Y, Sun Y, Jiang Y, Mater. Chem. Phys. 96, 2006, 234-239, doi.org/10.1016/j.matchemphys.2005.07.007

[23] Li Z, Wang Y, Liu J, Chen G, Li Y, Zhou C, Int. J. Hydrogen Energy 34, 2009, 147-152, doi.org/10.1016/j.ijhydene.2008.10.027

[24] Arean CO, Vinuela JSD, J. Solid State Chem. 60, 1985, 1-5, doi.org/10.1016/0022-4596(85)90156-2

[25] Arean CO, Martinez MLR, Arjona AM, Mater. Chem. Phys. 8, 1983, 443-450, doi.org/10.1016/0254-0584(83)90064-0

[26] Aupretre F, Descorme C, Duprez D, Casanave D, Uzio D, J. Catal. 233, 2005, 464-477, doi.org/10.1016/j.jcat.2005.05.007

[27] Augustin CO, Hema K, Berchmans LJ, Kalai Selvan R, Saraswathi R, Phys. Status Solidi 202, 2005, 1017-1024, doi.org/10.1002/pssa.200420027

[28] Chanda D, Hnát J, Paidar M, Bouzek K, Int. J. Hydrogen Energy 39, 2014, 5713-5722,

doi.org/10.1016/j.ijhydene.2014.01.141

[29] Landon J, Demeter E, Inoglu N, Keturakis C, Wachs IE, Vasic R, ACS Catal. 2, 2012, 1793-1801, doi: 10.1021/cs3002644

[30] Godinho MI, Catarino MA, Silva Pereira MI, Mendonça MH, Costa FM, Electrochim. Acta 47, 2002, 4307-4314, doi.org/10.1016/S0013-4686(02)00434-6

[31] Singh RN, Singh JP, Lal B, Thomas MJK, Bera S, Electrochim. Acta 51, 2006, 5515-5523, doi.org/10.1016/j.electacta.2006.02.028

[32] Rida K, Pena MA, Sastre E, Martinez-Arias A, J. Rare Earths 30, 2012, 210-216, doi.org/10.1016/S1002-0721(12)60025-8

[33] Devi PS, Rao MS, J. Anal. Appl. Pyrolysis 22, 1992, 187-195, doi.org/10.1016/0165-2370(92)85012-A

[34] Wang H, Zhu Y, Liu P, Yao W, J. Mater. Sci. 38, 2003, 1939-1943, doi.org/10.1023/A:1023504514207

[35] Marciuš M, Ristić M, Ivanda M, Musić S, J. Alloys Compd. 541, 2012, 238-243, doi.org/10.1016/j.jallcom.2012.07.021

[36] Kochur AG, Kozakov AT, Googlev KA, Kubrin SP, Nikolskii AV, Torgashev VI, J. Alloys Compd. 636, 2015, 241-248, doi.org/10.1016/j.jallcom.2015.02.150

[37] Ptak M, Mkaczka M, Pikul A, Tomaszewski PE, Hanuza J, J.Solid State Chem. 212, 2014, 218-226, doi.org/10.1016/j.jssc.2013.10.048

[38] Ragupathi C, Vijaya JJ, Kennedy LJ, J. Saudi Chem. Soc. 21, 2017, S231-S239, doi.org/10.1016/j.jscs.2014.01.006

[39] Bayal N, Jeevanandam P, J. Alloys Compd. 516, 2012, 27-32, doi.org/10.1016/j.jallcom.2011.11.080

[40] Anchieta CG, Tochetto L, Madalosso HB, Sulkovski RD, Serpa C, Mazutti MA, Almeida A.R.F, Gündel A, Foletto E.L, Ceramica 61, 2015, 477-481, doi.org/10.1590/0366-69132015613601925

[41] Preudhomme J, Tarte P, Spectrochim. Acta Part A Mol. Spectrosc. 27, 1971,1817-1835, doi.org/10.1016/0584-8539(71)80235-0

[42] Becheri A, Dürr M, Nostro PL, Baglioni P, J. Nanoparticle Res. 10, 2008, 679-689,

doi.org/10.1007/s11051-007-9318-3

[43] Jung GB, Huang TJ, Huang MH, Chang CL, J. Mater. Sci. 36, 2001, 5839-5844, doi.org/10.1023/A:1012964307388

[44] Garcia FAC, Silva JCM, Macedo JL, Dias JA, Dias SCL, Geraldo Filho N.R, Microporous Mesoporous Mater. 113, 2008, 562-574, doi.org/10.1016/j.micromeso.2007.12.017

[45] Li LF, Selloni A, ACS Catal. 4, 2014, 1148-1153, DOI: 10.1021/cs401245q

[46] Xiao C, Lu X, Zhao C, Chem. Commun. 50, 2014, 10122-10125, doi: 10.1039/C4CC04922E

[47] Burke MS, Enman LJ, Batchellor AS, Zou S, Boettcher SW, Chem. Mater. 27, 2015, 7549-7558, doi: 10.1021/acs.chemmater.5b03148

[48] Friebel D, Louie M. W., Bajdich M, Sanwald K. E., Cai Y, Wise A. M., Cheng M.J., Sokaras D., Weng T.C., Alonso-Mori R, Davis R.C., Bargar J.R., Nørskov J.K., Nilsson A., Bell A.T., J. Am. Chem. Soc. 137, 2015, 1305−1313, doi: 10.1021/ja511559d.

[49] Qi J, Zhang W, Xiang R, Liu K, Wang HY, Chen M, Han Y, Cao R, Adv.Sci. 2, 2015, 1500199-1500206, doi: 10.1002/advs.201500199.

How to cite this article:
TibermacineW, Omari M. Structural and electrochemical properties of Fe-doped $NiAl_2O_4$ oxides. J. Fundam. Appl. Sci., 2019, *11(1), 227-244.*